Published in final edited form as:
J Immunol. 2015 February 15; 194(4): 1467–1479. doi:10.4049/jimmunol.1402807.

IRF5 deficiency ameliorates lupus but promotes atherosclerosis and metabolic dysfunction in a mouse model of lupus-associated atherosclerosis

Amanda A. Watkins[*], **Kei Yasuda**[*], **Gabriella E. Wilson**[*], **Tamar Aprahamian**[*], **Yao Xie**[*], **Elena Maganto-Garcia**[‡], **Prachi Shukla**[*], **Lillian Oberlander**[*], **Bari Laskow**[*], **Hanni Menn-Josephy**[*], **Yuanyuan Wu**[†], **Pierre Duffau**[*], **Susan K. Fried**[†], **Andrew H. Lichtman**[‡], **Ramon G. Bonegio**[*], and **Ian R. Rifkin**[*]

[*]Renal Section, Department of Medicine, Boston University School of Medicine, Boston, MA, USA

[†]Endocrinology Section, Department of Medicine, Boston University School of Medicine, Boston, MA, USA

[‡]Vascular Research Division, Department of Pathology, Brigham and Women's Hospital, and Harvard Medical School, Boston, MA, USA

Abstract

Premature atherosclerosis is a severe complication of lupus and other systemic autoimmune disorders. Gain-of-function polymorphisms in interferon regulatory factor 5 (IRF5) are associated with an increased risk of developing lupus and IRF5 deficiency in lupus mouse models ameliorates disease. However, whether IRF5 deficiency also protects against atherosclerosis development in lupus is not known. Here we addressed this question using the *gld.apoE*$^{-/-}$ mouse model. IRF5 deficiency markedly reduced lupus disease severity. Unexpectedly, despite the reduction in systemic immune activation, IRF5-deficient mice developed increased atherosclerosis and also exhibited metabolic dysregulation characterized by hyperlipidemia, increased adiposity and insulin resistance. Levels of the atheroprotective cytokine IL-10 were reduced in aortae of IRF5-deficient mice and in vitro studies demonstrated that IRF5 is required for IL-10 production downstream of TLR7 and TLR9 signaling in multiple immune cell types. Chimera studies showed that IRF5 deficiency in bone marrow-derived cells prevents lupus development and contributes in part to the increased atherosclerosis. Notably, IRF5 deficiency in non-bone marrow-derived cells also contributes to the increased atherosclerosis through the generation of hyperlipidemia and increased adiposity. Together, our results reveal a protective role for IRF5 in lupus-associated atherosclerosis that is mediated through the effects of IRF5 in both immune and non-immune cells. These findings have implications for the proposed targeting of IRF5 in the treatment of autoimmune disease as global IRF5 inhibition may exacerbate cardiovascular disease in these patients.

[2] Address correspondence and reprint requests to Dr. Ian Rifkin, Renal Section, Department of Medicine, Boston University School of Medicine, EBRC 5th floor, 650 Albany Street, Boston, MA 02118 USA. Phone: 617-638-7325 Fax: 617-638-7326, irifkin@bu.edu.

Introduction

Systemic lupus erythematosus (SLE) is an autoimmune disease that is characterized by the loss of tolerance to nuclear self antigens, the production of pathogenic autoantibodies, and inflammation with damage to multiple organ systems (1). Premature atherosclerosis is a severe complication of SLE leading to appreciable morbidity and mortality from cardiovascular disease (2-4). Traditional (Framingham) risk factors contribute to atherosclerosis in SLE but do not explain the majority of the increased cardiovascular risk. After controlling for traditional risk factors, patients with SLE still have a substantial increased risk of cardiovascular disease (5). This has led to the concept that the autoimmune disease itself may be the strongest risk factor for cardiovascular disease in SLE. A number of previous studies have identified possible mechanisms whereby autoimmunity contributes to premature atherosclerosis (reviewed in (2, 4, 6). For example, it has been clearly demonstrated that immune system dysregulation and activation accelerates atherosclerosis in lupus-prone mice, with increased $CD4^+$ T cell and macrophage activation, type I interferon and impaired apoptotic cell clearance all involved in atherosclerosis pathogenesis (7-10). Thus, the chronic inflammation associated with SLE may be one important factor contributing to premature atherosclerosis in SLE, perhaps amplifying the chronic inflammation that underlies atherosclerosis pathogenesis in the general population (2-4, 11). Premature atherosclerosis is also a feature of other systemic autoimmune diseases including rheumatoid arthritis, vasculitis and psoriasis (12, 13).

Gain-of-function polymorphisms in the transcription factor interferon regulatory factor 5 (IRF5) are strongly associated in human genetic studies with an increased risk of developing a number of autoimmune diseases including SLE, scleroderma, Sjögren's disease, rheumatoid arthritis and inflammatory bowel disease (14, 15). IRF5 was originally identified as a transcription factor involved in the induction of type I interferons and pro-inflammatory cytokines by viral infection (16, 17) and subsequently was shown to play an important role in pro-inflammatory cytokine production following Toll-like receptor (TLR) signaling (18, 19). IRF5 also participates in signaling downstream of nucleotide-binding oligomerization domain 2 (NOD2) and Dectin-1 (20, 21), and in apoptotic pathways induced by viral infection, DNA damage, Fas ligand (FasL), or TRAIL (22-24). IRF5 promotes T helper 1 (Th1)/Th17-type immune responses and LPS-induced M1 macrophage polarization (25, 26). IRF5 deficiency ameliorates disease in a number of murine lupus models (27-32). For these reasons, IRF5 is being considered as a potential therapeutic target in SLE and other autoimmune diseases as well as in other inflammatory conditions such as post-myocardial infarction healing (14, 33). Thus, it is necessary to understand the role of IRF5 in atherosclerosis pathogenesis in the context of SLE in order to predict how such proposed IRF5 inhibitor treatment for SLE might impact the premature atherosclerosis that occurs in this disease.

We previously developed the *gld.apoE*$^{-/-}$ mouse model and have used it to study the interaction between atherosclerosis and SLE (7, 34, 35). The *gld* mutation is a point mutation in the gene encoding murine FasL and leads to the development of a mild form of spontaneous autoimmune disease on the C57BL/6 genetic background characterized by the production of low levels of autoantibodies and mild splenomegaly, lymphadenopathy and

glomerulonephritis (36-38). Apolipoprotein E-deficient ($apoE^{-/-}$) mice develop hypercholesterolemia and atherosclerosis (39). The combination of the *gld* mutation and apolipoprotein E deficiency in $gld.apoE^{-/-}$ mice results in more severe autoimmunity than is seen with the *gld* mutation alone and more severe atherosclerosis than is seen with apolipoprotein E deficiency alone (7).

In this report, we used the $gld.apoE^{-/-}$ mouse model to determine the role of IRF5 in lupus-associated atherosclerosis. We hypothesized that IRF5 deficiency would protect against atherosclerosis development by ameliorating lupus autoimmunity, thereby reducing the chronic inflammation associated with the autoimmune process. However we found that despite markedly reducing lupus disease severity, IRF5 deficiency unexpectedly led to an increase in atherosclerosis. Furthermore, the studies revealed an unanticipated role for IRF5 in maintaining metabolic homeostasis in that IRF5 deficiency resulted in hyperlipidemia, insulin resistance with hyperglycemia, hepatic steatosis and increased adiposity.

Materials and Methods

Mice

$Irf5^{-/-}$ mice backcrossed eight generations to C57BL/6 were obtained from T. Taniguchi (University of Tokyo, Tokyo, Japan) with permission from T. Mak (University of Toronto, Toronto, Ontario, Canada) (18). $Irf5^{-/-}$ mice were backcrossed three more generations to C57BL/6 and then intercrossed with $Fasl^{gld/gld}.apoE^{-/-}$ mice (referred to as $gld.apoE^{-/-}$ in this manuscript) on the C57BL/6 background (7) to generate IRF5 heterozygous ($Irf5^{+/-}$) $gld.apoE^{-/-}$ mice. Experimental mice were generated by breeding $Irf5^{+/-}$ $.gld.apoE^{-/-}$ mice to obtain $Irf5^{+/+}$, $Irf5^{+/-}$ and $Irf5^{-/-}$ $gld.apoE^{-/-}$ littermates. All mice used for breeding were screened for the Dock2 mutation (40, 41) and found to only have wild-type Dock2. Unless otherwise stated, we combined the data obtained from male and female littermates as we observed a similar qualitative effect of IRF5 deficiency in both genders. This could not be done in the case of body weight (Fig. 3) given the intrinsic differences in body weight between the genders. Animal protocols were approved by the Institutional Animal Care and Use Committee at Boston University.

Western diet administration and measurement of food consumption

Western diet containing cholesterol (0.2% total cholesterol), total fat (21% by weight; 42% kcal from fat), saturated fatty acids (>60% of total fatty acids), high sucrose (34% by weight) was purchased from Harlan Teklad (Cat. No. 88137). $Irf5^{+/+}.gld.apoE^{-/-}$, $Irf5^{+/-}.gld.apoE^{-/-}$ and $Irf5^{-/-}$ $.gld.apoE^{-/-}$ littermate mice were placed on western diet at 7 weeks of age and weighed weekly for 12 weeks. Littermate groups were separated into individual cages at the beginning of the 11^{th} week on western diet and food consumption by each individual mouse was measured over a period of 7 days to determine daily food consumption.

Bone marrow chimera studies

At 7 weeks of age male $Irf5^{+/+}$ $.gld.apoE^{-/-}$ and $Irf5^{-/-}$ $.gld.apoE^{-/-}$ bone marrow recipients were X-ray irradiated with 2 doses of 550 rads spaced three hours apart. Bone

marrow was harvested from age-matched male *Irf5*$^{+/+}$.*gld.apoE*$^{-/-}$ and *Irf5*$^{-/-}$.*gld.apoE*$^{-/-}$ donor mice and 5×10^5 bone marrow cells were administered to recipients via tail vein injection. Bone marrow recipients were given Sulfamethoxazole-Trimethoprim for three weeks and thereafter placed on western diet for 6-9 weeks and euthanized at 16-19 weeks of age.

PCR

The PCRs used to genotype *gld*, *apoE*$^{-/-}$, the Dock2 mutant and *Irf5*$^{-/-}$ were described previously (7, 27, 41).

Serological assays

Anti-nuclear autoantibody (ANA) titer was measured by immunofluorescence using slides coated with permeabilized human epithelial cells (HEp-2-coated-slides-INOVA Diagnostics, Inc. San Diego, California). Serially diluted mouse serum was incubated on HEp2 slides, washed and incubated with Alexa Fluor 568-conjugated goat anti-mouse IgG (1:100, Invitrogen). HEp2 slides were then washed, mounted and visualized as described below in the microscopy section. The ANA titer is taken as the last positive serum dilution. Serum triglyceride, total cholesterol, phospholipids and non-esterified free fatty acids were measured by the Mouse Metabolic Phenotyping Center, University of Cincinnati; U24 DK059630. Lipoprotein profiles were measured using fast performance liquid chromatography by the Mouse Metabolic Phenotyping Center, University of Cincinnati; U24 DK059630. Serum leptin, glucose, insulin and cytokine levels were measured by the Analytical Core at the Mouse Metabolic Phenotyping Center at the University of Massachusetts Medical Center. IL-10 in culture supernatant was measured by ELISA using the mouse BD OptEIA^{TM} Mouse IL-10 ELISA set according to the manufacturer's instructions (BD Biosciences,San Jose, CA).

Histology

Kidney sections were stained with hematoxylin and eosin (H & E) and evaluated in a blinded manner. Randomly selected areas of cortex were imaged as described below in the microscopy section. Fifty glomeruli from each animal were examined to determine the percentage of glomeruli with severe lesions (defined as glomerular crescents or areas of necrosis), mild lesions (defined as mesangial expansion) or no lesions. Crescents were identified by the presence of more than 3 palisading layers of cells in the extra-capillary space, and fibrinoid necrosis was identified by its classic eosinophillic and acellular appearance. Mesangial expansion was identified by prominence of the mesangial matrix as compared to mesangial matrix in normal glomeruli. Liver was fixed in 4% paraformaldehyde, paraffin-embedded, cut into 8 μm sections and stained with H & E. Severity of liver steatosis was quantified on coded samples by assessing visually the amount of lipid droplets present and scored on a scale of 0-3, with 0 being no lipid droplets and 3 being the largest amount of lipid droplets. Perigonadal fat pads were fixed in 4% formalin and stored in 1x PBS. Samples were sent to the Dana-Farber Harvard Cancer Center Pathology Core for embedding, sectioning and H & E staining.

Microscopy

Fixed and stained tissue sections were viewed using a Nikon Optiphot epifluorescent microscope and digitally photographed using an RT color spot camera (Diagnostic Instruments, Sterling Heights, MI) with Spot Advanced software version 4.0.9 (Diagnostic Instruments) except for stained aortic arches which were viewed using an Olympus SZXI6 microscope and digitally photographed using an Olympus Digital DP72 Camera (Japan) with CellSens Standard software version 1.11 (Olympus Corporation). Liver and aortic root sections were imaged at 4x. Liver and adipose tissue sections were imaged at 10x. Kidney sections and ANA were imaged at 20x.

Analysis of atherosclerosis

For aortic root analysis, the apex of the heart was cut at a 45 degree angle, and the cut side of the heart was placed on the bottom of a plastic cartridge filled with OCT. Correct placement of the cut heart was carried out so that the aortic root was parallel to the bottom of the plastic cartridge. The aortic arch was cut at the point at which it joins the heart. Hearts were snap-frozen in OCT in ice-cold methylbutane and dry ice. 8 μm serial aortic root sections were cut and slides were fixed in 4% paraformaldehyde. 24-30 aortic root sections per mouse heart were stained with Oil Red O and hematoxylin, and photographed. In a blinded manner, the average area of aortic lesions was quantified using Adobe Photoshop CS3.

For aortic arch analysis, the aortic arch from each mouse was fixed in 4% paraformaldehyde, cut longitudinally, pinned and stained with Oil Red O to detect lipid deposition. Aortic arches were photographed and in a blinded manner, the area of the total aortic arch and area stained positive for Oil Red O was quantified using Adobe Photoshop CS3 color range tool. The data is reported as average percentage of total aortic arch stained positive for Oil Red O in each experimental group.

Foam cell formation assay

Sera were collected from *Irf5*$^{+/+}$.*gld.apoE*$^{-/-}$ and *Irf5*$^{-/-}$.*gld.apoE*$^{-/-}$ mice that had been on western diet for 12 weeks. Peritoneal macrophages from C57BL/6 mice were seeded in tissue culture dishes in complete RPMI 1640 medium (10% fetal bovine serum, 2 mM L-glutamine, 100 U/ml penicillin and 100 μg/ml streptomycin) in 12 well flat-bottom plates and allowed to rest for 4-6 hours. Peritoneal macrophages were then treated with 5% *Irf5*$^{+/+}$.*gld.apoE*$^{-/-}$ or *Irf5*$^{-/-}$.*gld.apoE*$^{-/-}$ sera for 36 hours. The cells were then formalin fixed, stained with Oil Red O and images were photographed using a 20x objective lens. For each experimental condition, and in a blinded manner, the area of 20-25 macrophages was measured and the percentage of the area that was positive for Oil Red O was determined using the Adobe Photoshop CS3 color range tool. Data is reported as the average of three separate experiments using sera from three different *Irf5*$^{+/+}$.*gld.apoE*$^{-/-}$ and *Irf5*$^{-/-}$.*gld.apoE*$^{-/-}$ littermate groups.

Isolation of stromal vascular fraction (SVF) from perigonadal fat pad

Perigonadal fat pad was minced and digested in 0.5-1mL Collagenase Type I media (1x Collagenase Type I Worthington Cat. No 4196 370 units/mg, 1% bovine serum albumin in M199 media plus adenosine to a final concentration of 1 μM to inhibit lipolysis of adipocytes), CO2 -infused and incubated at 37°C for 45 minutes-1.5 hours. The SVF/ adipocyte mixture was diluted and passed through a 20 μm filter. After 10 minutes, adipocytes floated to the top and SVF cells were suspended in the layer below. The SVF was then removed using polyethylene tubing and a 18.5 gauge needle with syringe. The SVF was pelleted, treated with red blood cell lysis buffer, washed, resuspended in 3% FBS with 0.5M EDTA in PBS and counted. SVF isolation performed with the assistance of the Boston Nutrition Obesity Research Center.

Flow cytometry

SVF suspensions were labeled with a PE-Cy5-conjugated monoclonal antibody specific for F4/80 (IgG2a, Clone BM8; eBioscience, Inc., San Diego, California) or an isotype control (IgG2a) to identify adipose tissue macrophages. Immunoflourescence was measured using an LSRII (BD Bioscience). The data was analyzed using FlowJo software (Tree Star, Ashland, OR). Live cells within the SVF were gated based on FSC and SSC. The percent of maximum that was positive for F4/80 was quantified relative to isotype control.

Non-invasive magnetic resonance to assess body composition

Assessment of body composition (fat mass and lean tissue mass) was performed by non-invasive quantitative magnetic resonance (EchoMRI700) at the Metabolic Phenotyping Core at Boston University School of Medicine.

Glucose and insulin tolerance tests (GTT and ITT)

Irf5$^{+/+}$*.gld.apoE*$^{-/-}$, *Irf5*$^{+/-}$*.gld.apoE*$^{-/-}$ and *Irf5*$^{-/-}$*.gld.apoE*$^{-/-}$ littermate mice on western diet for 6-8 weeks were fasted for 6 hours and baseline blood glucose was measured using a glucometer (Accu-Chek Aviva system). Mice were given either an intraperitoneal glucose (1 g of glucose/kg of body weight) or insulin (0.75 units of insulin/kg body weight) injection. Blood glucose was measured at 15, 30, 45, 60, 90 and 120 minutes after intraperitoneal injection.

Preparation of cells for in vitro assays

To generate M-CSF bone marrow-derived macrophages (termed M-CSF macrophages), bone marrow cells from *Irf5*$^{+/+}$ and *Irf5*$^{-/-}$ C57BL/6 mice were seeded in tissue culture dishes in complete DMEM medium (10% fetal bovine serum, 2 mM L-glutamine, 100 U/ml penicillin and 100 μg/ml streptomycin) supplemented with 10% conditioned medium from L929 cells as the source of M-CSF. The cells were collected after 6 days and plated overnight at 1×10^6 cells/ml in flat bottom 96 well plates before stimulation.

To generate GM-CSF bone marrow-derived dendritic cells (termed GM-CSF DC) and GM-CSF bone marrow-derived macrophages (termed GM-CSF macrophages) (42) bone marrow cells were seeded at 0.5×10^6 cells/ml in complete RPMI 1640 together with 6.7 ng/ml

recombinant mouse GM-CSF (BD Biosciences). On day 6, the floating cells (GM-CSF DCs) (43) were collected and plated at 2×10^6 cells/ml in round bottom 96 well plates before stimulation. Adherent cells (GM-CSF macrophages) were collected by scraping and plated at 1×10^6 cells/ml overnight in flat bottom 96 well plates before stimulation, with duplicate wells for all stimulation conditions.

To generate Flt-3L bone marrow-derived dendritic cells (termed Flt-3L DC), bone marrow cells were seeded at 1.5×10^6 cells/ml in complete RPMI 1640 supplemented with 7.5% conditioned medium from B16 cells transfected with fml-like tyrosine kinase 3 ligand (Flt-3L). The Flt-3L B16 cells were originally made by Dr H. Chapman (44) and were provided by Dr U. Von Andrian (Harvard Medical School). The cells were used for experiments after 8 days, at which time 3×10^5 Flt-3L DCs were seeded in 96-well round-bottom plates and cultured in complete RPMI 1640 with the relevant stimuli in a total well volume of 200 μl.

To obtain B cells, spleen cells were incubated with anti-B220-biotin (BD Biosciences) for 15 min after treatment with red blood cell lysing buffer. The cells were washed with flow cytometry buffer (3% fetal bovine serum, 2 mM EDTA in PBS), incubated with streptavidin-magnetic particles (BD Biosciences) for 30 min and then purified using iMagnet (BD Biosciences). Four hundred thousand cells per well were seeded in 96-well flat-bottom plates.

In vitro immune cell activation

M-CSF macrophages, GM-CSF macrophages, GM-CSF dendritic cells, Flt-3L dendritic cells and splenic B cells from C57BL/6 WT and *Irf5*$^{-/-}$ mice were stimulated, or not stimulated, with the TLR2 ligand (S)-(2,3-bis(palmitoyloxy)-(2RS)-propyl)-N-palmityol-*R*-Cys-(S)-Ser(S)-Lys_4 –OH (Pam3Cys at 100-1000 ng/ml), the TLR3 ligand polyinosinic-polycytidylic acid (Poly I:C at 10 μg/ml), the TLR4 ligand LPS (100 ng/ml), the TLR7 ligands R848 (100 ng/ml) or R837 (0.3-1 μg/ml) and the TLR9 ligands unmethylated cytosine-guanine-rich DNA-B (CpG-B at 100 ng/ml) or CpG-A (100 ng/ml) (all from Invitrogen). Supernatants were collected after 24 hours, or after 5 days in the case of Flt3L dendritic cells, and IL-10 was measured by ELISA.

RNA isolation

Aortic arches and the SVF pellets isolated from perigonadal fat pads were snap frozen and stored at −80°C. Upon thawing, tissue or cell pellets were immediately resuspended in QIAzol (Qiagen) and lysed using the TissueLyser (Qiagen) or homogenized by vortexing. RNA was then isolated using either the RNeasy® Fibrous Tissue Mini Kit for aortic arch or the RNeasy® Mini Kit for SVF and resuspended in RNAse-free water (Qiagen). RNA yield was measured using a Nanodrop 2000 Spectrophotometer (Thermo Scientific).

Real-time PCR

RNA from the SVF of perigonadal fat and aortic arch was treated with DNase and reverse transcribed into cDNA using Thermoscript reverse transcriptase (Invitrogen). cDNA was diluted 1:100 and PCR was performed using Taqman primers specific for murine *Irf5, IL-10,*

IL-6 or *TNFα*. Data was analyzed using the $2^{-\Delta\Delta Ct}$ method and is expressed as 'Fold Change' (expression relative to housekeeping gene and normalized to reference sample).

Statistical analysis

For normally distributed data, groups were compared using either Student's *t* test or ANOVA. In cases where ANOVA was statistically significant, post-hoc comparison between groups was performed by Student's *t* test with Bonferroni correction for multiple comparisons. For data that was not normally distributed, the Mann-Whitney *U* test or one-way ANOVA on ranks was used. All statistics were performed using GraphPad Instat or SigmaPlot 12.5 (Systat, San Jose, USA) with $P < 0.05$ considered as statistically significant.

Results

IRF5 deficiency reduces autoimmune manifestations in gld.apoE$^{-/-}$ mice

We mated *Irf5* heterozygous (*Irf5*$^{+/-}$) *gld.apoE*$^{-/-}$ mice to generate *Irf5*$^{+/+}$*.gld.apoE*$^{-/-}$, *Irf5*$^{+/-}$*. gld.apoE*$^{-/-}$ and *Irf5*$^{-/-}$*.gld.apoE*$^{-/-}$ littermates and analyzed disease parameters in these experimental groups after 12 weeks on Western diet. All experiments were done with littermates to minimize any possible effects due to differences in gut microbiota, as the microbiome has recently been shown to substantially modify both autoimmune and metabolic responses (45-48).

As in other murine lupus models, autoimmune disease in the *gld.apoE*$^{-/-}$ model is characterized by splenomegaly, lymphadenopathy, anti-nuclear autoantibody (ANA) production and kidney disease (7). *Irf5*$^{+/+}$*.gld.apoE*$^{-/-}$ mice had splenomegaly and lymphadenopathy (Fig. 1A, B), elevated serum ANA titers (Fig. 1C) and renal disease (Fig. 1D, E). These features of lupus autoimmunity were all markedly reduced in *Irf5*$^{-/-}$*.gld.apoE*$^{-/-}$ littermates. In addition, serum levels of the pro-inflammatory cytokines IL-12p70, IFN-γ and TNF-α were lower in the *Irf5*$^{-/-}$*.gld.apoE*$^{-/-}$ mice (Fig. 1F). Notably, *Irf5*$^{+/-}$*.gld.apoE*$^{-/-}$ mice also exhibited markedly reduced disease manifestations indicating that loss of even a single allele of *Irf5* is sufficient to protect against the development of autoimmunity. These data demonstrate that IRF5 is required for lupus disease pathogenesis in the *gld.apoE*$^{-/-}$ model.

IRF5 deficiency promotes atherosclerosis and hyperlipidemia in gld.apoE−/− mice

To determine the role of IRF5 in atherosclerosis development, we evaluated atherosclerosis lesions using Oil Red O staining. Unexpectedly, *Irf5*$^{-/-}$*.gld.apoE*$^{-/-}$ mice had larger lesions in the aortic root and more extensive lesions in the aortic arch than *Irf5*$^{+/+}$*.gld.apoE*$^{-/-}$ littermates, both indicative of more severe atherosclerosis (Fig. 2A-C). As this result was the opposite of that predicted, we sought to identify possible mechanisms to explain this finding. We noted that the sera of the *Irf5*$^{-/-}$*.gld.apoE*$^{-/-}$ mice were more turbid than the sera of the *Irf5*$^{+/+}$*.gld.apoE*$^{-/-}$ littermates suggesting the presence of hyperlipidemia (Fig. 2D). This was confirmed with serum lipid measurements demonstrating increased serum levels of triglycerides, cholesterol, non-esterified fatty acids and phospholipids in the *Irf5*$^{-/-}$*.gld.apoE*$^{-/-}$ mice (Fig. 2E). Additional analysis showed increased levels of very low density lipoprotein (VLDL) and decreased levels of high density lipoprotein (HDL) in the

Irf5$^{-/-}$.*gld.apoE*$^{-/-}$ mice consistent with an atherogenic profile (Fig. 2F). To further evaluate the atherogenic capacity of the sera, we performed in vitro assays of foam cell generation. Foam cells form after macrophage uptake of lipoproteins in the subendothelium of atherosclerotic lesions and are thought to play a central role in atherosclerosis pathogenesis (49, 50). Sera from the *Irf5*$^{-/-}$.*gld.apoE*$^{-/-}$ mice were much more effective in inducing foam cell formation from C57BL/6 wildtype peritoneal macrophages (Fig. 2G) than sera from the *Irf5*$^{+/+}$.*gld.apoE*$^{-/-}$ mice. These data indicate that IRF5 deficiency promotes the development of atherosclerosis in *gld.apoE*$^{-/-}$ mice and that this might be due, at least in part, to an increase in the degree of hyperlipidemia.

IRF5 deficiency is associated with increased adipose tissue mass and inflammation in gld.apoE$^{-/-}$ mice

To determine whether IRF5 exerts other effects on metabolism we next evaluated food intake, weight gain and adipose tissue mass. There was no difference in food intake or weight gain between IRF5-sufficient and IRF5-deficient *gld.apoE*$^{-/-}$ littermates (Fig. 3A, B). However, despite the lack of difference in total body weight, *Irf5*$^{-/-}$.*gld.apoE*$^{-/-}$ mice had increased amounts of perigonadal and subcutaneous white fat (Fig. 3C). Adipocyte size was also increased (Fig. 3D). Serum leptin levels correlate with the mass of white adipose tissue (51) and were accordingly increased in the *Irf5*$^{-/-}$.*gld.apoE*$^{-/-}$ mice (Fig. 3E). To validate these findings, nuclear magnetic resonance (NMR) imaging was performed on a separate cohort of littermates and revealed a more than two-fold increase in fat mass in the *Irf5*$^{-/-}$.*gld.apoE*$^{-/-}$ mice (Fig. 3F, G). This was accompanied by a corresponding decrease in lean body mass in the *Irf5*$^{-/-}$.*gld.apoE*$^{-/-}$ mice.

Obesity is frequently accompanied by adipose tissue inflammation which is thought to play a role in atherosclerosis pathogenesis (52). To determine whether the increased adiposity was associated with increased adipose tissue inflammation we fractionated adipose tissue into adipocytes and the non-adipocyte stromal vascular fraction (SVF) and measured macrophage infiltration and pro-inflammatory cytokine production in the SVF. *Irf5*$^{-/-}$.*gld.apoE*$^{-/-}$ mice had an increased percentage of macrophages in the SVF compared to *Irf5*$^{+/+}$.*gld.apoE*$^{-/-}$ mice (Fig. 3H, I) and also increased expression of TNF-α with a trend towards an increase in IL-6 (Fig. 3J). Thus IRF5 deficiency results in both increased adipose tissue mass and increased adipose tissue inflammation in *gld.apoE*$^{-/-}$ mice. These effects of IRF5 deficiency on adipose tissue were not due to autoimmunity- or inflammation-induced cachexia in the *Irf5*$^{+/+}$.*gld.apoE*$^{-/-}$ mice as there was no difference in body weight between the experimental groups (Fig. 3B) and *Irf5*$^{+/+}$.*gld.apoE*−/− mice actually had a greater lean body mass than the *Irf5*$^{-/-}$.*gld.apoE*$^{-/-}$ mice (Fig 3F, G).

IRF5 deficiency leads to insulin resistance and hepatic steatosis in gld.apoE$^{-/-}$ mice

As increased fat mass and adipose tissue inflammation are linked to the development of diabetes we measured glucose levels in serum collected at the time of euthanasia. This showed that the *Irf5*$^{-/-}$.*gld.apoE*$^{-/-}$ mice had substantially elevated non-fasting serum glucose levels whereas those in the *Irf5*$^{+/+}$.*gld.apoE*$^{-/-}$ mice were normal (Fig. 4A). However, serum insulin levels were similar in the various experimental groups suggesting that the *Irf5*$^{-/-}$.*gld.apoE*$^{-/-}$ mice might be insulin-resistant (Fig. 4B). To test this

possibility, glucose and insulin tolerance tests were performed on additional littermate cohorts and these demonstrated that the *Irf5*$^{-/-}$.*gld.apoE*$^{-/-}$ mice were both glucose-intolerant and insulin-resistant (Fig. 4C, D). Hepatic steatosis can be a direct result of obesity-induced insulin-resistance and is also often associated with hypertriglyceridemia and hypercholesterolemia (53, 54). Liver histology revealed marked accumulation of lipid within hepatocytes of *Irf5*$^{-/-}$.*gld.apoE*$^{-/-}$ mice as compared with *Irf5*$^{+/+}$.*gld.apoE*$^{-/-}$ mice, consistent with hepatic steatosis (Fig. 4E, F). Taken together with the increased hyperlipidemia, these data demonstrate that IRF5 deficiency causes dysregulation of metabolic homeostasis in *gld.apoE*$^{-/-}$ mice resulting in features of metabolic syndrome.

IRF5 heterozygote gld.apoE$^{-/-}$ mice also exhibit metabolic dysregulation

Deficiency of a single allele of *Irf5* was sufficient to induce metabolic dysregulation. As compared with *Irf5*$^{+/+}$.*gld.apoE*$^{-/-}$ mice, *Irf5*$^{+/-}$.*gld.apoE*$^{-/-}$ mice had increased serum levels of triglycerides, cholesterol and phospholipids (Fig. 2E), increased perigonadal and subcutaneous white fat (Fig. 3C), and were glucose intolerant and insulin resistant (Fig. 4A-D). These metabolic parameters in *Irf5*$^{+/-}$.*gld.apoE*$^{-/-}$ mice were affected to a very similar extent as was seen in *Irf5*$^{-/-}$.*gld.apoE*$^{-/-}$ mice, suggesting that a certain threshold level of IRF5 is needed to protect against the development of metabolic dysregulation.

IRF5 expression in bone marrow-derived cells is required for the development of autoimmunity

IRF5 is most highly expressed in hematopoietic cell lineages, including B lymphocytes, monocytes, dendritic cells and macrophages (16, 18, 26, 55, 56). However, IRF5 transcript is also detected in non-hematopoietic tissue including muscle, liver and pre-adipocytes (16, 18, 22, 57).

To gain insight into which IRF5-expressing cells are responsible for the autoimmune, atherosclerosis and metabolic phenotypes observed, we performed bone marrow chimera studies. Seven week old *Irf5*$^{+/+}$.*gld.apoE*$^{-/-}$ and *Irf5*$^{-/-}$.*gld.apoE*$^{-/-}$ recipient mice were irradiated and reconstituted with bone marrow from either *Irf5*$^{+/+}$.*gld.apoE*$^{-/-}$ or *Irf5*$^{-/-}$.*gld.apoE*$^{-/-}$ age-matched mice. Mice were placed on western diet for 6-9 weeks starting 3 weeks after reconstitution and disease parameters were evaluated at 16-19 weeks of age. Statistical analysis was performed using 2-way analysis of variance to determine whether IRF5-expression in the donor (D) or in the recipient (R) was contributing to the disease parameter being evaluated.

Both *Irf5*$^{+/+}$ and *Irf5*$^{-/-}$ recipients reconstituted with *Irf5*$^{+/+}$ bone marrow developed splenomegaly, lymphadenopathy and high titer anti-nuclear autoantibodies (Fig. 5A-C). In contrast, *Irf5*$^{+/+}$ and *Irf5*$^{-/-}$ mice reconstituted with *Irf5*$^{-/-}$ bone marrow had spleen and lymph nodes of close to normal weight and only low level ANA titers comparable to that seen previously in *Irf5*$^{-/-}$.*gld.apoE*$^{-/-}$ mice. IRF5 deficiency in the recipients modestly reduced spleen size but did not affect lymph node size or ANA titer. Thus, the development of autoimmune disease is primarily dependent on IRF5 expression in bone-marrow-derived cells.

IRF5 expression in both bone marrow-derived and non-bone marrow-derived cells reduces atherosclerosis severity

We next measured atherosclerotic lesion size in the different bone marrow chimera groups. *Irf5*$^{-/-}$ recipient mice given *Irf5*$^{-/-}$ bone marrow developed substantially more atherosclerosis than *Irf5*$^{+/+}$ recipient mice given *Irf5*$^{+/+}$ bone marrow (Fig. 5D), confirming that IRF5 deficiency promotes atherosclerosis as previously shown (Fig. 2A-C). IRF5 deficiency in both the donor and the recipient mice contributed to the increased atherosclerosis although the more highly statistically significant contribution was seen with IRF5 deficiency in the recipients. The largest atherosclerotic lesions were seen in *Irf5*$^{-/-}$ recipient mice given *Irf5*$^{-/-}$ bone marrow consistent with the effects of IRF5 deficiency in bone marrow-derived and non-bone marrow-derived cells being additive. Thus, IRF5 expression in both bone marrow-derived and non-bone marrow-derived cells protects against the development of atherosclerosis in *gld.apoE*$^{-/-}$ mice.

IRF5 expression in non-bone marrow-derived cells plays the major role in reducing adipose tissue weight and the level of hyperlipidemia

IRF5 deficiency in recipient mice resulted in an increase in the amount of perigonadal and subcutaneous fat. This was most evident with *Irf5*$^{-/-}$ recipient mice given *Irf5*$^{+/+}$ bone marrow but was also seen with *Irf5*$^{-/-}$ recipient mice given *Irf5*$^{-/-}$ bone marrow (Fig. 5E). In contrast, IRF5 deficiency in donor mice did not result in a statistically significant increase in adipose tissue weight, although there was a strong trend towards such an increase.

Similarly, IRF5 deficiency in recipient mice resulted in an increase in the level of hyperlipidemia, with increases in triglycerides, cholesterol, non-esterified fatty acids and phospholipids being seen (Fig. 5F). This was seen with *Irf5*$^{-/-}$ recipient mice given either *Irf5*$^{+/+}$ or *Irf5*$^{-/-}$ bone marrow. IRF5 deficiency in donor mice also resulted in an increase in serum cholesterol levels but did not affect the levels of triglycerides, non-esterified fatty acids or phospholipids suggesting the possibility that cholesterol is being regulated through pathways distinct from that of the other lipids (Fig. 5F).

Taken together these data demonstrate that IRF5 deficiency in non-bone marrow-derived cells plays the major role in the increase in adipose tissue weight and hyperlipidemia observed in the *Irf5*$^{-/-}$*.gld.apoE*$^{-/-}$ mice, although IRF5 deficiency in bone marrow-derived cells plays a contributory role in serum cholesterol regulation and possibly also in the regulation of adipose tissue weight.

IL-10 expression is reduced in the aortae of Irf5$^{-/-}$.gld.apoE$^{-/-}$ mice and IRF5 is required for IL-10 production induced by TLR7 and TLR9 signaling in immune cells

The bone marrow chimera experiments demonstrated that IRF5 deficiency in both bone marrow-derived and non-bone marrow-derived cells promotes atherosclerosis development in the *Irf5*$^{-/-}$*.gld.apoE*$^{-/-}$ mice. They further demonstrated that the increased hyperlipidemia was due largely to IRF5 deficiency in non-bone marrow-derived cells providing a possible explanation for how IRF5 deficiency in non-bone marrow-derived cells might promote atherosclerosis. However, the chimera studies did not easily explain how IRF5 deficiency in bone marrow-derived cells might promote atherosclerosis. IL-10 is a

major anti-atherogenic cytokine and is thought to reduce atherosclerosis severity through a number of mechanisms (58-61), with leukocytes being the predominant producers of the IL-10 (62). We found that, in addition to reducing serum levels of pro-inflammatory cytokines as shown in Figure 1F, IRF5 deficiency also substantially reduced serum IL-10 levels in *gld.apoE*$^{-/-}$ mice on western diet for 12 weeks (Fig. 6A) and thus we hypothesized that IRF5 deficiency in immune (bone marrow-derived) cells might promote atheroscerosis by reducing IL-10 levels in the atherosclerotic lesions.

We measured IL-10 expression in the aortic arches of *Irf5*$^{+/+}$, *Irf5*$^{+/-}$ and *Irf5*$^{-/-}$*.gld.apoE*$^{-/-}$ mice by RT-PCR and found that IL-10 expression levels were markedly reduced in the *Irf5*$^{-/-}$*.gld.apoE*$^{-/-}$ mice (Fig. 6B). To determine whether IRF5 can regulate IL-10 at the cellular level, we stimulated a number of immune cell types in vitro with a panel of TLR ligands and measured IL-10 production. TLR7 and TLR9 ligands induced IL-10 production in bone marrow-derived M-CSF macrophages, GM-CSF macrophages, GM-CSF dendritic cells, Flt3L dendritic cells and primary splenic B cells and in all these cell types IL-10 production was largely IRF5-dependent (Fig. 6 C-G). TLR2 and TLR4 ligands also induced IL-10 production in these cell types but this was IRF5-independent. Thus IRF5 is required for IL-10 production downstream of TLR7 and TLR9 in multiple cell types. This is particularly intriguing in the context of atherosclerosis as both TLR7 and TLR9 deficiency have recently been shown to promote atherosclerosis in mouse models (63, 64).

Discussion

Premature atherosclerosis is a severe complication of SLE leading to appreciable morbidity and mortality from cardiovascular disease (2, 3). Gain-of-function polymorphisms in IRF5 are strongly associated with an increased risk of developing SLE and IRF5 inhibition is being considered as a therapeutic approach in SLE (14). However, the role of IRF5 in atherosclerosis pathogenesis is not known. We hypothesized that IRF5 deficiency would reduce atherosclerosis severity in the context of lupus for two main reasons. Firstly, the inflammation due to the active autoimmune process is thought to contribute to the premature atherosclerosis in SLE (2) and previous studies in other lupus mouse models suggested that IRF5 deficiency would reduce the active autoimmune process (27-32). Secondly, atherosclerosis itself, independently of systemic autoimmune disease, is driven by a Th1-skewed chronic inflammatory process in which M1-type macrophages play a dominant role (11), and IRF5 has been shown to promote both Th1 responses and M1-type macrophage development (25, 26). However we unexpectedly found that IRF5 deficiency in the *gld.apoE*$^{-/-}$ model, despite markedly reducing lupus autoimmunity and systemic inflammation, results in more severe atherosclerosis. In addition, IRF5 deficiency results in a more severe metabolic phenotype characterized by increased hyperlipidemia, insulin resistance with hyperglycemia, hepatic steatosis and increased adiposity. An additional surprising observation was that these effects on atherosclerosis and metabolism were driven not only by IRF5 deficiency in immune cells but also by IRF5 deficiency in non-immune cells.

The protective role of IRF5 in atherosclerosis seen in the *gld.apoE*$^{-/-}$ model may be mediated at least in part through TLRs. Although TLR2 and TLR4 promote atherosclerosis, TLR3, TLR7 and TLR9 appear to protect against atherosclerosis development. Deficiency of TLR2 or TLR4 in mouse atherosclerosis models results in a reduction in atherosclerosis lesion size (65, 66), whereas deficiency of TLR3, TLR7 or TLR9 results in an increase in atherosclerosis lesion size (63, 64, 67). The reasons for the differential effects of the cell surface TLRs, TLR2 and TLR4, and the nucleic-acid sensing TLRs, TLR3, TLR7 and TLR9, on atherosclerosis development remain incompletely understood although the nature of both the TLR agonist and the responding cell type are likely to play a role (68). IRF5 participates in signaling cascades downstream of TLR3, TLR4, TLR5, TLR7 and TLR9 (18, 19, 41, 69, 70) and thus the increased atherosclerosis we observed in the IRF5-deficient *gld.apoE*$^{-/-}$ mice could be a result of altered functional outcomes following TLR3, TLR7 or TLR9 activation, leading to a loss of the atheroprotective effect normally mediated by these nucleic-acid sensing TLRs. Extracellular endogenous RNA and DNA are present within atherosclerotic lesions (63, 71). Apoptotic cell death is an important feature of atherosclerotic plaques and may provide the endogenous RNA or DNA ligands required for activation of TLR7 and TLR9 (71, 72). Such apoptotic cell death may exert beneficial effects in early atherosclerosis by the induction of the anti-atherogenic cytokines IL-10 and TGF-β but detrimental effects in advanced atherosclerosis through necrotic cell accumulation and the induction of pro-inflammatory responses (72).

Indeed we found that production of IL-10 induced by TLR7 and TLR9 activation is markedly reduced in the absence of IRF5 in multiple immune cell types and that IL-10 expression is reduced in the aortae of IRF5-deficient *gld.apoE*$^{-/-}$ mice. In contrast, we found no effect of IRF5 deficiency on IL-10 production induced by TLR2 and TLR4 activation and a previous study found that IRF5 deficiency actually led to an increase in IL-10 production in M1-type macrophages following TLR4 activation (26). Thus IRF5 is required for IL-10 production preferentially downstream of TLR7 and TLR9 activation and this may be one mechanism whereby IRF5 deficiency in immune cells promotes atherosclerosis, as IL-10 is the major anti-inflammatory cytokine responsible for protection against atherosclerosis (58-60).

An additional mechanism whereby IRF5 deficiency promotes atherosclerosis in our model is through the induction of hyperlipidemia. IRF5 deficiency resulted in a marked increase in serum VLDL levels and a reduction in serum HDL, a serum lipid profile that would be expected to be pro-atherogenic (73, 74). Accordingly sera from IRF5-deficient *gld.apoE*$^{-/-}$ mice induced the formation of foam cells from macrophages to a substantially greater extent than sera from IRF5-sufficient *gld.apoE*$^{-/-}$ mice. The increase in hyperlipidemia was due predominantly to IRF5 deficiency in non-bone marrow derived cells demonstrating that the serum lipid alterations were largely independent of lupus disease severity, as the lupus phenotype was dependent on IRF5 expression in bone marrow-derived cells. Further work will be needed to identify the non-immune cell type in which IRF5 acts to regulate these metabolic effects. The three major metabolically active tissues regulating serum lipid levels are liver, adipose tissue and the intestine whereas skeletal muscle is more important for maintaining glucose homeostasis (75, 76). In the initial IRF5 reports, it was shown that IRF5

is expressed in skeletal muscle but not in liver (16, 18). A subsequent study demonstrated IRF5 expression in the liver although it was not determined whether IRF5 was expressed in hepatocytes or in non-hepatocyte cell populations in the liver, such as Kupffer cells and sinusoidal epithelial cells (22). IRF5 is expressed only at a very low level in purified isolated adipocytes from C57BL/6 mice on a regular chow diet (57), however we have found that IRF5 expression is strongly upregulated in purified adipocytes from C57BL/6 mice on high fat diet (data not shown). This is consistent with published studies showing increased IRF5 expression in unfractionated adipose tissue from mice on high-fat diet (77). Very little is known about the function of IRF5 in skeletal myocytes, hepatocytes, adipocytes or in the lipid-regulating cells of the intestine.

Fas deficiency reduces adipose tissue weight and adipocyte size without affecting total body weight in C57BL/6 mice fed a high fat diet (78). Fas deficiency also protects against the deterioration of glucose homeostasis induced by high-fat diet, protects against hepatic steatosis and reduces adipose tissue inflammation (78). *gld.apoE*$^{-/-}$ mice are deficient in functional FasL and are thus unable to signal through Fas. This likely contributes to the reduced fat mass, small adipocyte size and normal glucose homeostasis observed in the IRF5-sufficient *gld.apoE*$^{-/-}$ mice on Western diet. These protective effects of FasL deficiency were not evident in *gld.apoE*$^{-/-}$ mice deficient in IRF5 which exhibited increased fat mass, enlarged adipocytes, reduced lean body mass and impaired glucose tolerance. FasL and TRAIL have opposing effects on metabolism in vivo with Fas/FasL deficiency resulting in a favorable metabolic phenotype (as detailed above) and TRAIL deficiency resulting in an unfavorable metabolic phenotype with hypercholesterolemia, adipocyte hypertrophy and impaired glucose tolerance (79). As FasL signaling is absent in *gld.apoE*$^{-/-}$ mice the effects of TRAIL signaling may be more apparent. As IRF5 participates in both Fas ligand and TRAIL-induced signaling in terms of apoptosis induction (22, 23) it is conceivable that IRF5 also participates in FasL and TRAIL-induced signaling in terms of metabolic regulation. If that is the case then IRF5 deficiency may have particularly marked metabolic effects in *gld.apoE*$^{-/-}$ mice. Further studies will be needed to determine how IRF5 deficiency impacts metabolism in mice with intact Fas/FasL signaling.

Previous studies have shown that IRF5 is required for disease development in a number of different mouse lupus models although interpretation of these studies was complicated by the possible presence of the Dock2 mutation in the IRF5 knockout mouse line used to generate the experimental mice (40, 41). In this study we have confirmed an important role for IRF5 in the pathogenesis of the lupus phenotype in a mouse model and have further demonstrated for the first time that IRF5 expression in bone marrow-derived cells is necessary and sufficient to promote this phenotype. It will be important in future studies to identify the specific IRF5-expressing immune cell type(s) responsible for promoting lupus pathogenesis and preventing atherosclerosis development because, if they are different, it would be preferable to target IRF5 inhibition only to the cell type driving lupus pathogenesis. Cell specific inhibition in vivo may be feasible as recently shown for IRF5 in macrophages (33).

In summary, we found that despite markedly reducing lupus disease severity, IRF5 deficiency led to an increase in atherosclerosis as well as metabolic dysregulation

characterized by increased hyperlipidemia, insulin resistance, hepatic steatosis and increased adiposity. This was due to distinct roles of IRF5 in both immune and non-immune cells. These findings have implications for the treatment of autoimmune diseases such as lupus where IRF5 inhibition is being considered as a therapeutic approach, as global IRF5 inhibition could potentially exacerbate cardiovascular disease in these patients.

Acknowledgements

We thank Tadatsugu Tanaguchi and Tak Mak for providing the IRF5-deficient mice. We thank Jeffrey Browning, Neil Ruderman, Tom Balon and Vassilis Zannis for helpful discussion. We thank Guneet Kochar, Rocco Richards, Mi-Jeong Lee, Mike Kirber and Panagiotis Fotakis for technical assistance. We thank the Boston University Flow Cytometry Core Facility for assistance with flow cytometry.

1. This work was supported by the following National Institutes of Health grants: P01 AR050256 (I.R.R), 1K01AR060857-01 (K.Y.), K01AR055965-01A1 (T.A.), R01 DK090558 (R.G.B.), A.A.W. was supported by the Research Training in Nephrology T32 Grant (5T32DK007053) and the Research Training in Immunology T32 Grant (AI007309-23) from the National Institutes of Health. S.K.F and Y.W. are members of Boston Nutrition Obesity Research Center supported by P30 DK46200.

3. Abbreviations

ANA	anti-nuclear autoantibody
DC	dendritic cell
FasL	Fas ligand
IRF5	interferon regulatory factor-5
SLE	Systemic lupus erythematosus
SVF	stromal vascular fraction

References

1. Liu Z, Davidson A. Taming lupus-a new understanding of pathogenesis is leading to clinical advances. Nat Med. 2012; 18:871–882. [PubMed: 22674006]
2. Skaggs BJ, Hahn BH, McMahon M. Accelerated atherosclerosis in patients with SLE--mechanisms and management. Nat Rev Rheumatol. 2012; 8:214–223. [PubMed: 22331061]
3. Nikpour M, Gladman DD, Urowitz MB. Premature coronary heart disease in systemic lupus erythematosus: what risk factors do we understand? Lupus. 2013; 22:1243–1250. [PubMed: 24097996]
4. Kahlenberg JM, Kaplan MJ. Mechanisms of premature atherosclerosis in rheumatoid arthritis and lupus. Annu Rev Med. 2013; 64:249–263. [PubMed: 23020882]
5. Esdaile JM, Abrahamowicz M, Grodzicky T, Li Y, Panaritis C, du Berger R, Cote R, Grover SA, Fortin PR, Clarke AE, Senecal JL. Traditional Framingham risk factors fail to fully account for accelerated atherosclerosis in systemic lupus erythematosus. Arthritis Rheum. 2001; 44:2331–2337. [PubMed: 11665973]
6. Wade NS, Major AS. The problem of accelerated atherosclerosis in systemic lupus erythematosus: insights into a complex co-morbidity. Thromb Haemost. 2011; 106:849–857. [PubMed: 21979131]
7. Aprahamian T, Rifkin I, Bonegio R, Hugel B, Freyssinet JM, Sato K, Castellot JJ Jr. Walsh K. Impaired clearance of apoptotic cells promotes synergy between atherogenesis and autoimmune disease. J Exp Med. 2004; 199:1121–1131. [PubMed: 15096538]
8. Stanic AK, Stein CM, Morgan AC, Fazio S, Linton MF, Wakeland EK, Olsen NJ, Major AS. Immune dysregulation accelerates atherosclerosis and modulates plaque composition in systemic lupus erythematosus. Proc Natl Acad Sci U S A. 2006; 103:7018–7023. [PubMed: 16636270]

9. Gautier EL, Huby T, Ouzilleau B, Doucet C, Saint-Charles F, Gremy G, Chapman MJ, Lesnik P. Enhanced immune system activation and arterial inflammation accelerates atherosclerosis in lupus-prone mice. Arterioscl Throm Vasc Biol. 2007; 27:1625–1631.
10. Thacker SG, Zhao W, Smith CK, Luo W, Wang H, Vivekanandan-Giri A, Rabquer BJ, Koch AE, Pennathur S, Davidson A, Eitzman DT, Kaplan MJ. Type I interferons modulate vascular function, repair, thrombosis, and plaque progression in murine models of lupus and atherosclerosis. Arthritis Rheum. 2012; 64:2975–2985. [PubMed: 22549550]
11. Libby P, Lichtman AH, Hansson GK. Immune effector mechanisms implicated in atherosclerosis: from mice to humans. Immunity. 2013; 38:1092–1104. [PubMed: 23809160]
12. Hollan I, Meroni PL, Ahearn JM, Cohen Tervaert JW, Curran S, Goodyear CS, Hestad KA, Kahaleh B, Riggio M, Shields K, Wasko MC. Cardiovascular disease in autoimmune rheumatic diseases. Autoimmun Rev. 2013; 12:1004–1015. [PubMed: 23541482]
13. Mason JC, Libby P. Cardiovascular disease in patients with chronic inflammation: mechanisms underlying premature cardiovascular events in rheumatologic conditions. Eur Heart J. 2014 doi: 10.1093/eurheartj/ehu403.
14. Lazzari E, Jefferies CA. IRF5-mediated signaling and implications for SLE. Clin Immunol. 2014; 153:343–52. [PubMed: 24928322]
15. Kottyan LC, Zoller EE, Bene J, Lu X, Kelly JA, Rupert AM, Lessard CJ, Vaughn SE, Marion M, Weirauch MT, Namjou B, Adler A, Rasmussen A, Glenn S, Montgomery CG, Hirschfield GM, Xie G, Coltescu C, Amos C, Li H, Ice JA, Nath SK, Mariette X, Rischmueller M, Lester S, Brun JG, Goransson LG, Harboe E, Omdal R, Cunninghame-Graham DS, Vyse T, Miceli-Richard C, Brennan MT, Lessard JA, Wahren-Herlenius M, Kvarnstrom M, Illei GG, Witte T, Jonsson R, Eriksson P, Nordmark G, Anaya JM, Rhodus NL, Segal BM, Merrill JT, James JA, Guthridge JM, Scofield RH, Alarcon-Riquelme M, Bae SC, Boackle SA, Criswell LA, Gilkeson G, Kamen DL, Jacob CO, Kimberly R, Brown E, Edberg J, Alarcon GS, Reveille JD, Vila LM, Petri M, Ramsey-Goldman R, Freedman BI, Niewold T, Stevens AM, Tsao BP, Ying J, Mayes MD, Gorlova OY, Wakeland W, Radstake T, Martin E, Martin J, Siminovitch K, Moser Sivils KL, Gaffney PM, Langefeld CD, Harley JB, Kaufman KM. The IRF5-TNPO3 association with systemic lupus erythematosus (SLE) has two components that other autoimmune disorders variably share. Hum Mol Genet. 2014 doi:10.1093/hmg/ddu455.
16. Barnes BJ, Moore PA, Pitha PM. Virus-specific activation of a novel interferon regulatory factor, IRF-5, results in the induction of distinct interferon alpha genes. J Biol Chem. 2001; 276:23382–23390. [PubMed: 11303025]
17. Barnes BJ, Kellum MJ, Field AE, Pitha PM. Multiple regulatory domains of IRF-5 control activation, cellular localization, and induction of chemokines that mediate recruitment of T lymphocytes. Mol Cell Biol. 2002; 22:5721–5740. [PubMed: 12138184]
18. Takaoka A, Yanai H, Kondo S, Duncan G, Negishi H, Mizutani T, Kano S, Honda K, Ohba Y, Mak TW, Taniguchi T. Integral role of IRF-5 in the gene induction programme activated by Toll-like receptors. Nature. 2005; 434:243–249. [PubMed: 15665823]
19. Schoenemeyer A, Barnes BJ, Mancl ME, Latz E, Goutagny N, Pitha PM, Fitzgerald KA, Golenbock DT. The interferon regulatory factor, IRF5, is a central mediator of toll-like receptor 7 signaling. J Biol Chem. 2005; 280:17005–17012. [PubMed: 15695821]
20. Pandey AK, Yang Y, Jiang Z, Fortune SM, Coulombe F, Behr MA, Fitzgerald KA, Sassetti CM, Kelliher MA. NOD2, RIP2 and IRF5 play a critical role in the type I interferon response to Mycobacterium tuberculosis. PLoS Pathog. 2009; 5:e1000500. [PubMed: 19578435]
21. del Fresno C, Soulat D, Roth S, Blazek K, Udalova I, Sancho D, Ruland J, Ardavin C. Interferon-beta production via Dectin-1-Syk-IRF5 signaling in dendritic cells is crucial for immunity to C. albicans. Immunity. 2013; 38:1176–1186.
22. Couzinet A, Tamura K, Chen HM, Nishimura K, Wang Z, Morishita Y, Takeda K, Yagita H, Yanai H, Taniguchi T, Tamura T. A cell-type-specific requirement for IFN regulatory factor 5 (IRF5) in Fas-induced apoptosis. Proc Natl Acad Sci U S A. 2008; 105:2556–2561. [PubMed: 18268344]
23. Hu G, Barnes BJ. IRF-5 is a mediator of the death receptor-induced apoptotic signaling pathway. J Biol Chem. 2009; 284:2767–2777. [PubMed: 19028697]

24. Yanai H, Chen HM, Inuzuka T, Kondo S, Mak TW, Takaoka A, Honda K, Taniguchi T. Role of IFN regulatory factor 5 transcription factor in antiviral immunity and tumor suppression. Proc Natl Acad Sci U S A. 2007; 104:3402–3407. [PubMed: 17360658]
25. Negishi H, Yanai H, Nakajima A, Koshiba R, Atarashi K, Matsuda A, Matsuki K, Miki S, Doi T, Aderem A, Nishio J, Smale ST, Honda K, Taniguchi T. Cross-interference of RLR and TLR signaling pathways modulates antibacterial T cell responses. Nat Immunol. 2012; 13:659–666. [PubMed: 22610141]
26. Krausgruber T, Blazek K, Smallie T, Alzabin S, Lockstone H, Sahgal N, Hussell T, Feldmann M, Udalova IA. IRF5 promotes inflammatory macrophage polarization and TH1-TH17 responses. Nat Immunol. 2011; 12:231–238. [PubMed: 21240265]
27. Richez C, Yasuda K, Bonegio RG, Watkins AA, Aprahamian T, Busto P, Richards RJ, Liu CL, Cheung R, Utz PJ, Marshak-Rothstein A, Rifkin IR. IFN regulatory factor 5 is required for disease development in the FcgammaRIIB−/−Yaa and FcgammaRIIB−/− mouse models of systemic lupus erythematosus. J Immunol.184: 796-806. 2010
28. Savitsky DA, Yanai H, Tamura T, Taniguchi T, Honda K. Contribution of IRF5 in B cells to the development of murine SLE-like disease through its transcriptional control of the IgG2a locus. Proc Natl Acad Sci U S A. 2010; 107:10154–10159. [PubMed: 20479222]
29. Tada Y, Kondo S, Aoki S, Koarada S, Inoue H, Suematsu R, Ohta A, Mak TW, Nagasawa K. Interferon regulatory factor 5 is critical for the development of lupus in MRL/lpr mice. Arthritis Rheum. 2011; 63:738–748. [PubMed: 21305501]
30. Feng D, Yang L, Bi X, Stone RC, Patel P, Barnes BJ. Irf5-deficient mice are protected from pristane-induced lupus via increased Th2 cytokines and altered IgG class switching. Eur J Immunol. 2012; 42:1477–1487. [PubMed: 22678902]
31. Xu Y, Lee PY, Li Y, Liu C, Zhuang H, Han S, Nacionales DC, Weinstein J, Mathews CE, Moldawer LL, Li SW, Satoh M, Yang LJ, Reeves WH. Pleiotropic IFN-dependent and -independent effects of IRF5 on the pathogenesis of experimental lupus. J Immunol.188: 4113-4121. 2012
32. Yasuda K, Watkins AA, Kochar GS, Wilson GE, Laskow B, Richez C, Bonegio RG, Rifkin IR. Interferon regulatory factor-5 deficiency ameliorates disease severity in the MRL/lpr mouse model of lupus in the absence of a mutation in DOCK2. PLoS One. 2014; 9:e103478. [PubMed: 25076492]
33. Courties G, Heidt T, Sebas M, Iwamoto Y, Jeon D, Truelove J, Tricot B, Wojtkiewicz G, Dutta P, Sager HB, Borodovsky A, Novobrantseva T, Klebanov B, Fitzgerald K, Anderson DG, Libby P, Swirski FK, Weissleder R, Nahrendorf M. In vivo silencing of the transcription factor IRF5 reprograms the macrophage phenotype and improves infarct healing. J Am Coll Cardiol. 2013; 63:1556–1566. [PubMed: 24361318]
34. Aprahamian T, Bonegio R, Rizzo J, Perlman H, Lefer DJ, Rifkin IR, Walsh K. Simvastatin treatment ameliorates autoimmune disease associated with accelerated atherosclerosis in a murine lupus model. J Immunol. 2006; 177:3028–3034. [PubMed: 16920939]
35. Aprahamian T, Bonegio RG, Richez C, Yasuda K, Chiang LK, Sato K, Walsh K, Rifkin IR. The peroxisome proliferator-activated receptor gamma agonist rosiglitazone ameliorates murine lupus by induction of adiponectin. J Immunol. 2009; 182:340–346. [PubMed: 19109165]
36. Takahashi T, Tanaka M, Brannan CI, Jenkins NA, Copeland NG, Suda T, Nagata S. Generalized lymphoproliferative disease in mice, caused by a point mutation in the Fas ligand. Cell. 1994; 76:969–976. [PubMed: 7511063]
37. Cohen PL, Eisenberg RA. Lpr and gld: single gene models of systemic autoimmunity and lymphoproliferative disease. Annu Rev Immunol. 1991; 9:243–269. [PubMed: 1910678]
38. Izui S, Kelley VE, Masuda K, Yoshida H, Roths JB, Murphy ED. Induction of various autoantibodies by mutant gene lpr in several strains of mice. J Immunol. 1984; 133:227–233. [PubMed: 6609979]
39. Plump AS, Smith JD, Hayek T, Aalto-Setala K, Walsh A, Verstuyft JG, Rubin EM, Breslow JL. Severe hypercholesterolemia and atherosclerosis in apolipoprotein E-deficient mice created by homologous recombination in ES cells. Cell. 1992; 71:343–353. [PubMed: 1423598]

40. Purtha WE, Swiecki M, Colonna M, Diamond MS, Bhattacharya D. Spontaneous mutation of the Dock2 gene in Irf5−/− mice complicates interpretation of type I interferon production and antibody responses. Proc Natl Acad Sci U S A. 2012; 109:E898–904. [PubMed: 22431588]
41. Yasuda K, Nundel K, Watkins AA, Dhawan T, Bonegio RG, Ubellacker JM, Marshak-Rothstein A, Rifkin IR. Phenotype and function of B cells and dendritic cells from interferon regulatory factor 5-deficient mice with and without a mutation in DOCK2. Int Immunol. 2013; 25:295–306. [PubMed: 23291967]
42. Hamilton JA. Colony-stimulating factors in inflammation and autoimmunity. Nat Rev Immunol. 2008; 8:533–544. [PubMed: 18551128]
43. Inaba K, Inaba M, Romani N, Aya H, Deguchi M, Ikehara S, Muramatsu S, Steinman RM. Generation of large numbers of dendritic cells from mouse bone marrow cultures supplemented with granulocyte/macrophage colony-stimulating factor. J Exp Med. 1992; 176:1693–1702. [PubMed: 1460426]
44. Shi GP, Villadangos JA, Dranoff G, Small C, Gu L, Haley KJ, Riese R, Ploegh HL, Chapman HA. Cathepsin S required for normal MHC class II peptide loading and germinal center development. Immunity. 1999; 10:197–206. [PubMed: 10072072]
45. Vijay-Kumar M, Aitken JD, Carvalho FA, Cullender TC, Mwangi S, Srinivasan S, Sitaraman SV, Knight R, Ley RE, Gewirtz AT. Metabolic syndrome and altered gut microbiota in mice lacking Toll-like receptor 5. Science. 2010; 328:228–231. [PubMed: 20203013]
46. Henao-Mejia J, Elinav E, Jin C, Hao L, Mehal WZ, Strowig T, Thaiss CA, Kau AL, Eisenbarth SC, Jurczak MJ, Camporez JP, Shulman GI, Gordon JI, Hoffman HM, Flavell RA. Inflammasome-mediated dysbiosis regulates progression of NAFLD and obesity. Nature. 2012; 482:179–185. [PubMed: 22297845]
47. Elinav E, Strowig T, Kau AL, Henao-Mejia J, Thaiss CA, Booth CJ, Peaper DR, Bertin J, Eisenbarth SC, Gordon JI, Flavell RA. NLRP6 inflammasome regulates colonic microbial ecology and risk for colitis. Cell. 2011; 145:745–757. [PubMed: 21565393]
48. Yurkovetskiy L, Burrows M, Khan AA, Graham L, Volchkov P, Becker L, Antonopoulos D, Umesaki Y, Chervonsky AV. Gender bias in autoimmunity is influenced by microbiota. Immunity. 2013; 39:400–412. [PubMed: 23973225]
49. Tabas I. Macrophage death and defective inflammation resolution in atherosclerosis. Nat Rev Immunol. 2010; 10:36–46. [PubMed: 19960040]
50. Moore KJ, Sheedy FJ, Fisher EA. Macrophages in atherosclerosis: a dynamic balance. Nat Rev Immunol. 2013; 13:709–721. [PubMed: 23995626]
51. Beltowski J. Leptin and atherosclerosis. Atherosclerosis. 2006; 189:47–60. [PubMed: 16580676]
52. Fantuzzi G, Mazzone T. Adipose tissue and atherosclerosis: exploring the connection. Arterioscl Throm Vasc Biol. 2007; 27:996–1003.
53. Browning JD, Horton JD. Molecular mediators of hepatic steatosis and liver injury. J Clin Invest. 2004; 114:147–152. [PubMed: 15254578]
54. Choi SH, Ginsberg HN. Increased very low density lipoprotein (VLDL) secretion, hepatic steatosis, and insulin resistance. Trends Endocrinol Metab: TEM. 2011; 22:353–363.
55. Krausgruber T, Saliba D, Ryzhakov G, Lanfrancotti A, Blazek K, Udalova IA. IRF5 is required for late-phase TNF secretion by human dendritic cells. Blood. 2010; 115:4421–4430. [PubMed: 20237317]
56. Stone RC, Feng D, Deng J, Singh S, Yang L, Fitzgerald-Bocarsly P, Eloranta ML, Ronnblom L, Barnes BJ. Interferon regulatory factor 5 activation in monocytes of systemic lupus erythematosus patients is triggered by circulating autoantigens independent of type I interferons. Arthritis Rheum. 2012; 64:788–798. [PubMed: 21968701]
57. Eguchi J, Yan QW, Schones DE, Kamal M, Hsu CH, Zhang MQ, Crawford GE, Rosen ED. Interferon regulatory factors are transcriptional regulators of adipogenesis. Cell Metab. 2008; 7:86–94. [PubMed: 18177728]
58. Kleemann R, Zadelaar S, Kooistra T. Cytokines and atherosclerosis: a comprehensive review of studies in mice. Cardiovasc Res. 2008; 79:360–376. [PubMed: 18487233]
59. Ait-Oufella H, Taleb S, Mallat Z, Tedgui A. Recent advances on the role of cytokines in atherosclerosis. Arterioscler Throm Vasc Biol. 2011; 31:969–979.

60. McLaren JE, Michael DR, Ashlin TG, Ramji DP. Cytokines, macrophage lipid metabolism and foam cells: implications for cardiovascular disease therapy. Prog Lipid Res. 2011; 50:331–347. [PubMed: 21601592]
61. Han X, Kitamoto S, Lian Q, Boisvert WA. Interleukin-10 facilitates both cholesterol uptake and efflux in macrophages. J Biol Chem. 2009; 284:32950–32958. [PubMed: 19776020]
62. Potteaux S, Esposito B, van Oostrom O, Brun V, Ardouin P, Groux H, Tedgui A, Mallat Z. Leukocyte-derived interleukin 10 is required for protection against atherosclerosis in low-density lipoprotein receptor knockout mice. Arterioscler Throm Vasc Biol. 2004; 24:1474–1478.
63. Salagianni M, Galani IE, Lundberg AM, Davos CH, Varela A, Gavriil A, Lyytikainen LP, Lehtimaki T, Sigala F, Folkersen L, Gorgoulis V, Lenglet S, Montecucco F, Mach F, Hedin U, Hansson GK, Monaco C, Andreakos E. Toll-like receptor 7 protects from atherosclerosis by constraining "inflammatory" macrophage activation. Circulation. 2012; 126:952–962. [PubMed: 22787112]
64. Koulis C, Chen YC, Hausding C, Ahrens I, Kyaw TS, Tay C, Allen T, Jandeleit-Dahm K, Sweet MJ, Akira S, Bobik A, Peter K, Agrotis A. Protective role for Toll-like receptor-9 in the development of atherosclerosis in apolipoprotein E-deficient mice. Arterioscler Throm Vasc Biol. 2014; 34:516–525.
65. Michelsen KS, Wong MH, Shah PK, Zhang W, Yano J, Doherty TM, Akira S, Rajavashisth TB, Arditi M. Lack of Toll-like receptor 4 or myeloid differentiation factor 88 reduces atherosclerosis and alters plaque phenotype in mice deficient in apolipoprotein E. Proc Natl Acad Sci U S A. 2004; 101:10679–10684. [PubMed: 15249654]
66. Mullick AE, Tobias PS, Curtiss LK. Modulation of atherosclerosis in mice by Toll-like receptor 2. J Clin Invest. 2005; 115:3149–3156. [PubMed: 16211093]
67. Cole JE, Navin TJ, Cross AJ, Goddard ME, Alexopoulou L, Mitra AT, Davies AH, Flavell RA, Feldmann M, Monaco C. Unexpected protective role for Toll-like receptor 3 in the arterial wall. Proc Natl Acad Sci U S A. 2011; 108:2372–2377. [PubMed: 21220319]
68. Cole JE, Kassiteridi C, Monaco C. Toll-like receptors in atherosclerosis: a 'Pandora's box' of advances and controversies. Trend Pharmacol Sci. 2013; 34:629–636.
69. Yasuda K, Richez C, Maciaszek JW, Agrawal N, Akira S, Marshak-Rothstein A, Rifkin IR. Murine dendritic cell type I IFN production induced by human IgG-RNA immune complexes is IFN regulatory factor (IRF)5 and IRF7 dependent and is required for IL-6 production. J Immunol. 2007; 178:6876–6885. [PubMed: 17513736]
70. Paun A, Reinert JT, Jiang Z, Medin C, Balkhi MY, Fitzgerald KA, Pitha PM. Functional characterization of murine interferon regulatory factor 5 (IRF-5) and its role in the innate antiviral response. J Biol Chem. 2008; 283:14295–14308. [PubMed: 18332133]
71. Doring Y, Manthey HD, Drechsler M, Lievens D, Megens RT, Soehnlein O, Busch M, Manca M, Koenen RR, Pelisek J, Daemen MJ, Lutgens E, Zenke M, Binder CJ, Weber C, Zernecke A. Auto-antigenic protein-DNA complexes stimulate plasmacytoid dendritic cells to promote atherosclerosis. Circulation. 2012; 125:1673–1683. [PubMed: 22388324]
72. Van Vre EA, Ait-Oufella H, Tedgui A, Mallat Z. Apoptotic cell death and efferocytosis in atherosclerosis. Arterioscler Thromb Vasc Biol. 2012; 32:887–893. [PubMed: 22328779]
73. Carmena R, Duriez P, Fruchart JC. Atherogenic lipoprotein particles in atherosclerosis. Circulation. 2004; 109:III2–7. [PubMed: 15198959]
74. Moller DE, Kaufman KD. Metabolic syndrome: a clinical and molecular perspective. Annu Rev Med. 2005; 56:45–62. [PubMed: 15660501]
75. Saltiel AR, Kahn CR. Insulin signalling and the regulation of glucose and lipid metabolism. Nature. 2001; 414:799–806. [PubMed: 11742412]
76. Abumrad NA, Davidson NO. Role of the gut in lipid homeostasis. Physiol Rev. 2012; 92:1061–1085. [PubMed: 22811425]
77. Kwon EY, Shin SK, Cho YY, Jung UJ, Kim E, Park T, Park JH, Yun JW, McGregor RA, Park YB, Choi MS. Time-course microarrays reveal early activation of the immune transcriptome and adipokine dysregulation leads to fibrosis in visceral adipose depots during diet-induced obesity. BMC genomics. 2012; 13:450. [PubMed: 22947075]

78. Wueest S, Rapold RA, Schumann DM, Rytka JM, Schildknecht A, Nov O, Chervonsky AV, Rudich A, Schoenle EJ, Donath MY, Konrad D. Deletion of Fas in adipocytes relieves adipose tissue inflammation and hepatic manifestations of obesity in mice. J Clin Invest. 2010; 120:191–202. [PubMed: 19955656]

79. Harith HH, Morris MJ, Kavurma MM. On the TRAIL of obesity and diabetes. Trends Endocrinol Metab: TEM. 2013; 24:578–587.

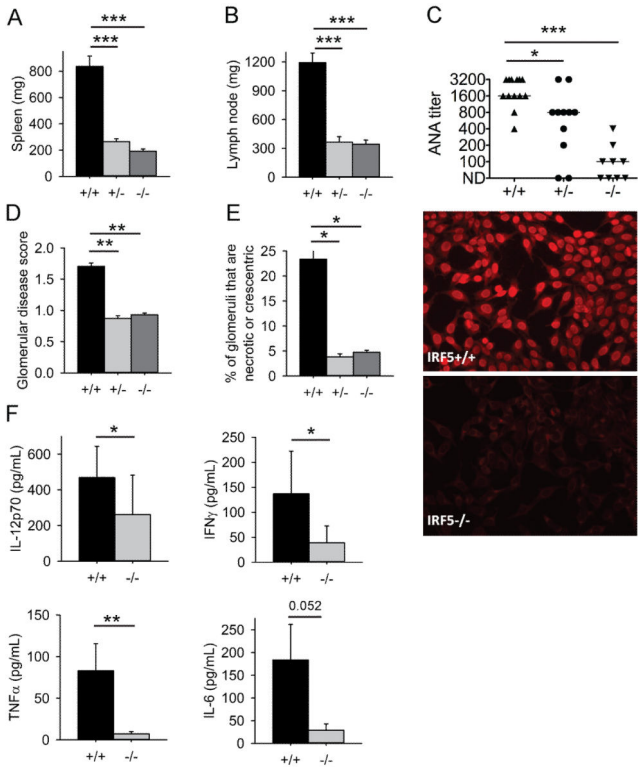

FIGURE 1.

IRF5 deficiency reduces lupus disease severity. Male and female *gld.apoE*$^{-/-}$ mice were euthanized at 19 weeks of age after 12 weeks on western diet. **(A)** Spleen and **(B)** lymph node weights from male and female *Irf5*$^{+/+}$ (n=27), *Irf5*$^{+/-}$(n=28) and *Irf5*$^{-/-}$(n=24) *gld.apoE*$^{-/-}$ littermate mice were measured. **(C)** Anti-nuclear autoantibody (ANA) titers in sera from *Irf5*$^{+/+}$ (n=13), *Irf5*$^{+/-}$ (n=11) and *Irf5*$^{-/-}$(n=9) *gld.apoE*$^{-/-}$ littermate mice were measured by immunofluorescence on HEp2 cells. Representative ANA immunofluorescence staining with sera from *Irf5*$^{+/+}$ and *Irf5*$^{-/-}$ *gld.apoE*$^{-/-}$ mice at a dilution of 1:100 is shown in the right-hand panels at 20x magnification. **(D)** Glomerular disease score and **(E)** the average percentage of glomeruli per kidney that are necrotic or crescentic was measured in kidney sections from *Irf5*$^{+/+}$ (n=15), *Irf5*$^{+/-}$ (n=9), and *Irf5*$^{-/-}$(n=15) *gld.apoE*$^{-/-}$ littermate mice. **(F)** Serum IL-12p70, TNFα, IFNγ and IL-6 cytokine levels from *Irf5*$^{+/+}$ (n=9) and *Irf5*$^{-/-}$(n=9) *gld.apoE*$^{-/-}$ littermate mice were measured by Luminex. Error bars represent the mean and SEM. (A-E) 2-way ANOVA and (F) Mann-Whitney *U* test. * p< 0.05, ** p< 0.01, *** p<0.001.

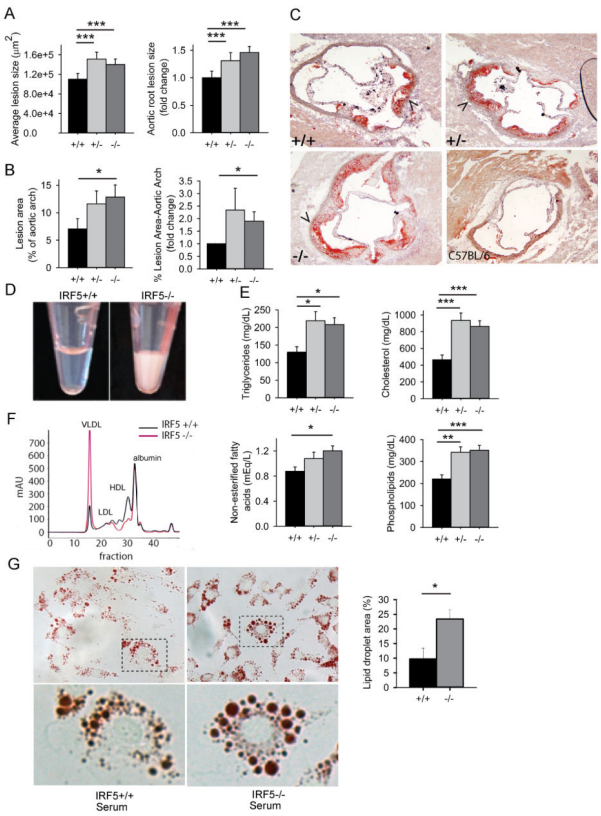

FIGURE 2.

IRF5-deficient *gld.apoE*$^{-/-}$ mice develop more severe atherosclerosis and increased hyperlipidemia**. (A-F)** Male and female *gld.apoE*$^{-/-}$ mice were euthanized at 19 weeks of age after 12 weeks on western diet and samples collected for analysis. **(A)** Serial aortic root sections from *Irf5*$^{+/+}$ (n=12), *Irf5*$^{+/-}$ (n=8) and *Irf5*$^{-/-}$ (n=14) *gld.apoE*$^{-/-}$ littermate mice were stained with Oil Red O to detect lipid deposition in atherosclerotic lesions and the lesion area was quantified. Left panel: Average aortic root lesion size. Right panel: The Y-axis represents the fold change of aortic root lesion area in *Irf5*$^{+/-}$ and *Irf5*$^{-/-}$ *gld.apoE*$^{-/-}$ mice relative to the *Irf5*$^{+/+}$ *gld.apoE*$^{-/-}$ littermate control. **(B)** Left panel: Percentage of aortic arch stained positive for Oil Red O from *Irf5*$^{+/+}$ (n=6), *Irf5*$^{+/-}$ (n=6) and *Irf5*$^{-/-}$ (n=7) *gld.apoE*$^{-/-}$ littermate mice. Right panel: The Y-axis represents the fold change of percentage of aortic arch stained positive for Oil Red O in *Irf5*$^{+/-}$ and *Irf5*$^{-/-}$ *gld.apoE*$^{-/-}$ mice relative to the *Irf5*$^{+/+}$ *gld.apoE*$^{-/-}$ littermate control. **(C)** Representative images of Oil Red O-stained aortic roots from *Irf5*$^{+/+}$, *Irf5*$^{+/-}$ and *Irf5*$^{-/-}$ *gld.apoE*$^{-/-}$ mice with arrowheads designating atherosclerotic lesions. An Oil Red O-stained aortic root from a C57BL/6 mouse not on western diet is shown as a reference. **(D)** Representative images of sera from *Irf5*$^{+/+}$ and *Irf5*$^{-/-}$ *gld.apoE*$^{-/-}$ littermates. **(E)** Levels of triglycerides, total cholesterol, non-esterified fatty acids and phospholipids in the sera of *Irf5*$^{+/+}$ (n=18), *Irf5*$^{+/-}$ (n=15), and *Irf5*$^{-/-}$ (n=19) *gld.apoE*$^{-/-}$ littermate mice. **(F)** Lipoprotein profiles from pooled sera of three *Irf5*$^{+/+}$ *gld.apoE*$^{-/-}$ and three *Irf5*$^{-/-}$ *gld.apoE*$^{-/-}$ mice. **(G)** Foam cell formation assay in vitro. Peritoneal macrophages from C57BL/6 mice were treated with 5% serum from *Irf5*$^{+/+}$ and *Irf5*$^{-/-}$ *gld.apoE*$^{-/-}$ mice for 36 hours and then stained with Oil Red

O. Representative high resolution images were taken using a 20x objective lens and digitally magnified by 5x (upper panels) and 15x (lower panels). The percentage of macrophage cell area positive for Oil Red O was quantified and is shown in the right panel. Error bars represent the mean and SEM of three separate experiments using sera from three different *Irf5*$^{+/+}$ and *Irf5*$^{-/-}$ *gld.apoE*$^{-/-}$ littermate groups. (A, B) The severity of atherosclerosis was ranked in *Irf5*$^{+/+}$, *Irf5*$^{+/-}$ and *Irf5*$^{-/-}$ *gld.apoE*$^{-/-}$ littermates housed in the same cage and the ranks were analyzed by 1-way ANOVA. (E) 2-way ANOVA, (G) Student's *t* test (two-sided). * $p < 0.05$, ** $p < 0.01$, *** $p < 0.001$.

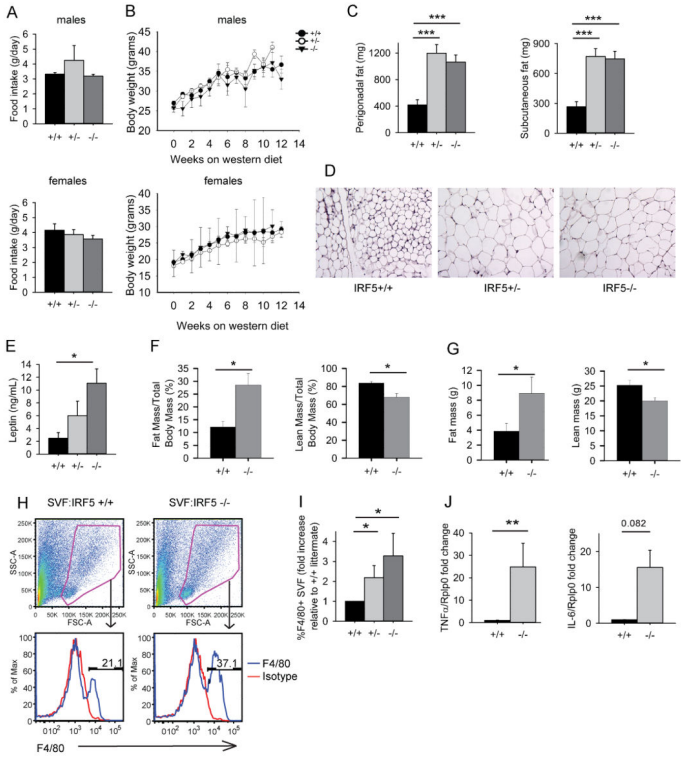

FIGURE 3.

IRF5 deficiency increases adipose tissue mass and inflammation. **(A)** Average amount of food consumed per day by *Irf5*$^{+/+}$ (n=9), *Irf5*$^{+/-}$ (n=3) and *Irf5*$^{-/-}$ (n=7) *gld.apoE*$^{-/-}$ male mice (top panel) and *Irf5*$^{+/+}$ (n=9), *Irf5*$^{+/-}$ (n=7) and *Irf5*$^{-/-}$ (n=13) *gld.apoE*$^{-/-}$ female littermate mice (bottom panel). **(B)** Body weight over time of *Irf5*$^{+/+}$ (n=11), *Irf5*$^{+/-}$ (n=15) and *Irf5*$^{-/-}$ (n=10) *gld.apoE*$^{-/-}$ - male mice (top panel) and *Irf5*$^{+/+}$ (n=10), *Irf5*$^{+/-}$ (n=15) and *Irf5*$^{-/-}$ (n=10) *gld.apoE*$^{-/-}$ female mice (bottom panel) on western diet for 12 weeks. **(C-E)** Male and female *gld.apoE*$^{-/-}$ mice were euthanized at 19 weeks of age after 12 weeks on western diet and samples collected for analysis. **(C)** Perigonadal fat and subcutaneous fat weights in *Irf5*$^{+/+}$ (n=25-26), *Irf5*$^{+/-}$ (n=27) and *Irf5*$^{-/-}$ (n=21-24) *gld.apoE*$^{-/-}$ littermate mice. **(D)** Representative images of H&E stained perigonadal fat pads from *Irf5*$^{+/+}$, *Irf5*$^{+/-}$ and *Irf5*$^{-/-}$*gld.apoE*$^{-/-}$ mice. 4x magnification. **(E)** Leptin levels in sera of *Irf5*$^{+/+}$ (n=4), *Irf5*$^{+/-}$ (n=3) and *Irf5*$^{-/-}$ (n=7) *gld.apoE*$^{-/-}$ littermate mice. **(F and G)** Nuclear magnetic imaging (NMR) studies performed on separate cohorts of *Irf5*$^{+/+}$ (n=4) and *Irf5*$^{-/-}$ (n=4) *gld.apoE*$^{-/-}$ female littermate mice after 12 weeks on western diet. **(F)** Percentage of body mass that is fat (left panel) and percentage of body mass that is lean (right panel). **(G)** Total fat mass (left panel) and total lean mass (right panel). **(H-I)** Stromal vascular fraction (SVF) of adipose tissue from *Irf5*$^{+/+}$ (n=7), *Irf5*$^{+/-}$ (n=5) and *Irf5*$^{-/-}$ (n=4) *gld.apoE*$^{-/-}$ male littermate mice after 12 weeks on western diet. **(H)** Representative dot plots showing live cell gate (top panels) and representative histograms of F4/80^{+} macrophages in SVF (bottom panels). **(I)** Percentage of F4/80^{+} macrophages in SVF relative to *Irf5*$^{+/+}$.*gld.apoE*$^{-/-}$ littermate, quantitated by flow cytometry. **(J)** TNFα and IL-6 expression in SVF of adipose tissue from *Irf5*$^{+/+}$ (n=6) and *Irf5*$^{-/-}$ (n=5) *gld.apoE*$^{-/-}$ male

littermate mice after 12 weeks on western diet measured by RT-PCR. Data are expressed as the average fold change of TNFα and IL-6 expression in SVF of adipose tissue from *Irf5*$^{-/-}$*.gld.apoE*$^{-/-}$ mice relative to the *Irf5*$^{+/+}$ *.gld.apoE*$^{-/-}$ littermate control. (C, E, I) 2-way ANOVA, (F, G) Student's *t* test (two-sided), (J) Mann-Whitney *U* Test. Error bars represent the mean and SEM. * $p < 0.05$, ** $p < 0.01$, *** $p < 0.001$.

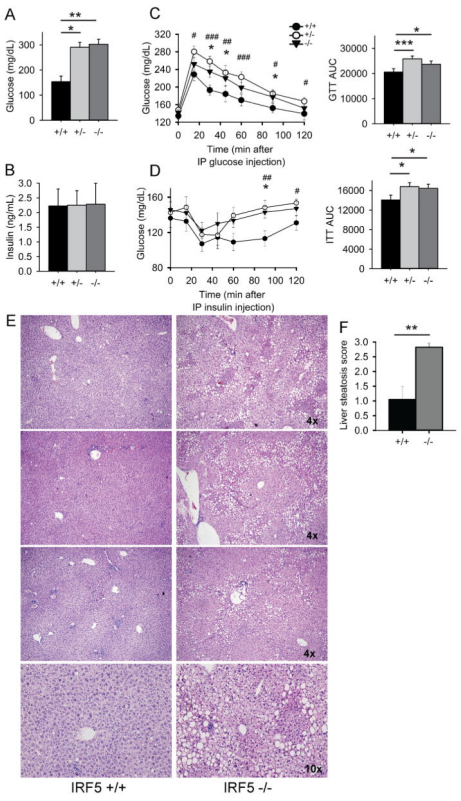

FIGURE 4.

IRF5 deficiency leads to insulin-resistance and liver steatosis in *gld.apoE*$^{-/-}$ mice. **(A and B)** Male and female *gld.apoE*$^{-/-}$ mice were euthanized at 19 weeks of age after 12 weeks on western diet and samples collected for analysis. **(A)** Glucose levels and **(B)** insulin levels in sera of *Irf5*$^{+/+}$ (n=5), *Irf5*$^{+/-}$ (n=4) and *Irf5*$^{-/-}$ (n=7) *gld.apoE*$^{-/-}$ mice. **(C)** Glucose tolerance tests (GTT) and **(D)** Insulin tolerance tests (ITT) were performed on male *Irf5*$^{+/+}$ (n=14-15), *Irf5*$^{+/-}$(n=16-17) and *Irf5*$^{-/-}$ (n=12-13) *gld.apoE*$^{-/-}$ littermate mice on western diet for 6-8 weeks. Time-course data is shown in the left hand panels and total area under the curve (AUC) is shown in the right hand panels. Error bars represent the mean and SEM. **(E)** H & E stained liver sections from three separate pairs of *Irf5*$^{+/+}$*gld.apoE*$^{-/-}$ and *Irf5*$^{-/-}$ *gld.apoE*$^{-/-}$ littermate mice on western diet for 12 weeks. Top 6 panels: 4x magnification; Bottom 2 panels: 10x magnification of top 2 panels. **(F)** Severity of liver steatosis was scored in liver sections from *Irf5*$^{+/+}$ (n=5) and *Irf5*$^{-/-}$(n=7) *gld.apoE*$^{-/-}$ littermate mice. (A,C,D) 2-way ANOVA. # denotes comparison *Irf5*$^{+/+}$ and *Irf5*$^{+/-}$ *gld.apoE*$^{-/-}$ littermate mice whereas * denotes comparison between *Irf5*$^{+/+}$ and *Irf5*$^{-/-}$ *gld.apoE*$^{-/-}$ littermate mice. (F) Student's *t* test (two-sided). *,# $p < 0.05$, **,## $p < 0.01$, ***,### $p < 0.001$.

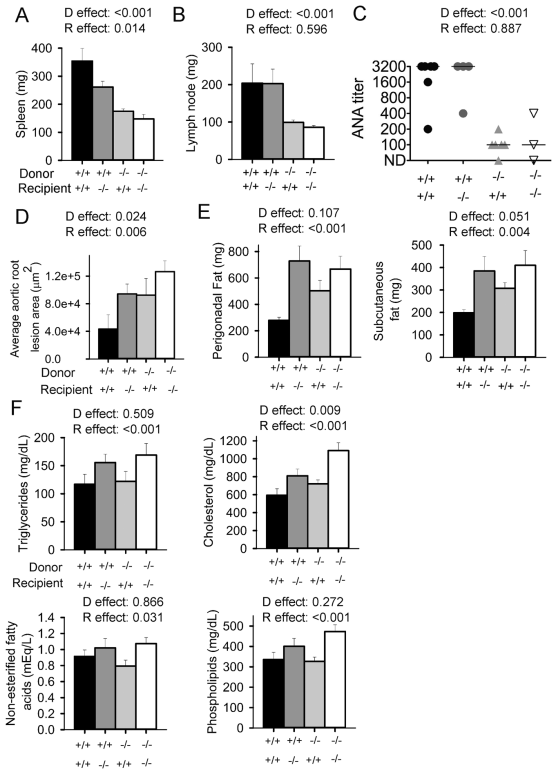

FIGURE 5.

The effects of Irf5 expression in bone marrow-derived and non-bone marrow-derived cells on disease parameters in *gld.apoE*$^{-/-}$ mice. *Irf5*$^{+/+}$*.gld.apoE*$^{-/-}$ and *Irf5*$^{-/-}$*.gld.apoE*$^{-/-}$ recipients were lethally irradiated and then reconstituted with bone marrow from either *Irf5*$^{+/+}$*gld.apoE*$^{-/-}$ or *Irf5*$^{-/-}$ *gld.apoE*$^{-/-}$ donor mice. Mice were placed on western diet for 6-9 weeks and disease parameters were analyzed at 16-19 weeks of age. **(A)** spleen and **(B)** cervical lymph node weights: $^{+/+}\rightarrow^{+/+}$ (n=8), $^{+/+}\rightarrow^{-/-}$ (n=5-6), $^{-/-}\rightarrow^{+/+}$ (n=9) and $^{-/-}\rightarrow^{-/-}$ (n=9). **(C)** Serum anti-nuclear autoantibody (ANA) titers: $^{+/+}\rightarrow^{+/+}$ (n=6), $^{+/+}\rightarrow^{-/-}$ (n=4), $^{-/-}\rightarrow^{+/+}$ (n=6) and $^{-/-}\rightarrow^{-/-}$ (n=3). **(D)** Serial aortic root sections were stained with Oil Red O to detect lipid deposition and the aortic root lesion size was quantitated: $^{+/+}\rightarrow^{+/+}$ (n=3), $^{+/+}\rightarrow^{-/-}$ (n=4), $^{-/-}\rightarrow^{+/+}$ (n=4) and $^{-/-}\rightarrow^{-/-}$ (n=4). **(E)** Perigonadal and subcutaneous fat pad weights: $^{+/+}\rightarrow^{+/+}$ (n=8), $^{+/+}\rightarrow^{-/-}$ (n=6), $^{-/-}\rightarrow^{+/+}$ (n=9) and $^{-/-}\rightarrow^{-/-}$ (n=10). **(F)** Serum triglyceride, cholesterol, non-esterified free fatty acid and phospholipid levels: $^{+/+}\rightarrow^{+/+}$ (n=8-10), $^{+/+}\rightarrow^{-/-}$ (n=7-10), $^{-/-}\rightarrow^{+/+}$ (n=6-9) and $^{-/-}\rightarrow^{-/-}$ (n=8-9). Error bars represent the mean and SEM. 2-way ANOVA P values are shown for the effect of IRF5 deficiency in the donor (D) and the effect of IRF5 deficiency in the recipient (R).

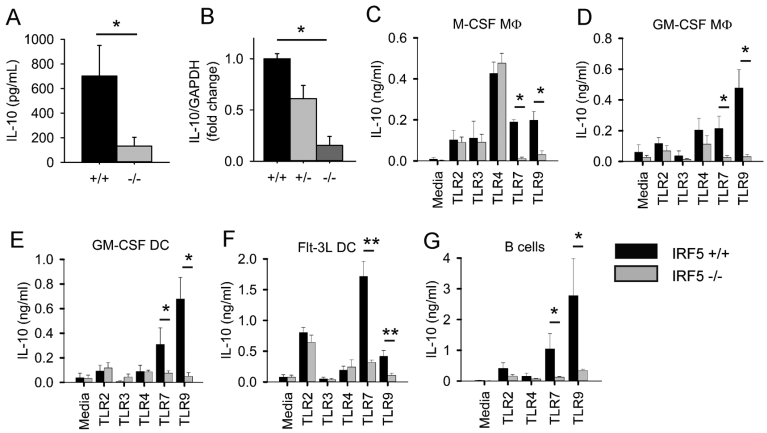

FIGURE 6.

IRF5 is required for IL-10 production induced by TLR7 and TLR9 signaling in immune cells. **(A)** Serum IL-10 cytokine levels from *Irf5*$^{+/+}$ (n=9) and *Irf5*$^{-/-}$(n=9) *gld.apoE*$^{-/-}$ littermate mice were measured by Luminex. **(B)** IL-10 gene expression in aortic arches of male and female *Irf5*$^{+/+}$ (n=7-8), *Irf5*$^{+/-}$ (n=6-7) and *Irf5*$^{-/-}$ (n=8) *gld.apoE*$^{-/-}$ mice after 12 weeks on western diet. Data are expressed as the average fold change of IL-10 expression in *Irf5*$^{+/-}$ and *Irf5*$^{-/-}$*.gld.apoE*$^{-/-}$ mice relative to the *Irf5*$^{+/+}$ *.gld.apoE*$^{-/-}$ littermate control. **(C)** Bone marrow-derived M-CSF macrophages, **(D)** GM-CSF macrophages, **(E)** GM-CSF dendritic cells, **(F)** Flt3 ligand dendritic cells and **(G)** splenic B cells from C57BL/6 WT and IRF5$^{-/-}$ mice were stimulated, or not stimulated (media), with the TLR2 ligand Pam3Cys (100-1000 ng/ml), the TLR3 ligand Poly(I:C) (10 μg/ml), the TLR4 ligand LPS (100 ng/ml), the TLR7 ligands R848 (100 ng/ml) or R837 (0.3-1 μg/ml) and the TLR9 ligands CpG-B (100 ng/ml) or CpG-A (100 ng/ml). Supernatants were collected after 24 hours, or after 5 days in the case of Flt3 dendritic cells, and IL-10 was measured by ELISA. Data represent the mean and SEM of 3-6 independent experiments for each cell type. Mann-Whitney *U* Test for all except (B) which was 1-way ANOVA. * $p < 0.05$, ** $p < 0.01$.